Oxoammonium-Catalyzed Ether Oxidation *via* Hydride Abstraction: Methodology Development and Mechanistic Investigation using Paramagnetic Relaxation Enhancement NMR

Yukun Cheng, Jonas Rein, Nguyen Le and Song Lin*

Department of Chemistry and Chemical Biology, Cornell University, Ithaca, New York 14853, United States

ABSTRACT: Hydride abstraction represents a promising yet underexplored approach in the functionalization of C–H bonds. In this work, we report the oxidation of α-C–H bonds of ethers *via* oxoammonium catalysis using 3-chloroperbenzoic acid (*m*CPBA) as the terminal chemical oxidant or by means of electrochemistry. Mechanistic studies revealed intricate equilibria and interconversion events between various catalytic intermediates in the presence of *m*CPBA, which alone however was incompetent to drive catalytic turnover. The addition of a small amount of strong acid $HNTf_2$ or weakly coordinating salt $NaSbF_6$ turned on catalytic turnover and promoted ether oxidation with excellent efficiency. NMR experiments leveraging paramagnetic relaxation enhancement effect allowed for quantification of open-shell catalytic intermediates in real time during the reaction course, which aided the identification of catalyst resting states and elucidation of reaction mechanisms.

INTRODUCTION

The direct functionalization of C–H bonds has now been widely recognized as an enabling tool in organic synthesis, medicinal chemistry, and materials science.[1] In addition to powerful strategies made possible by transition metal catalysis,[2] the use of small organic molecules as catalysts or promoters for C–H functionalization has attracted broad interest from the synthetic community in recent years. In this context, the mechanism of C–H cleavage can be generally categorized into three classes via protic,[3] radical,[4] and hydridic[5] pathways (Scheme 1A). The radical and hydridic pathways are both effective for activating non-acidic C–H bonds, but they often exhibit distinct selectivity, largely influenced by the stability of the resulting radical and carbocation intermediates, respectively, which are often quantified by bond dissociation energy ($\Delta H_{homolytic}$) and hydricity ($\Delta H_{hydridic}$).[5b,6] While the former approach via hydrogen atom transfer (HAT) has been extensively explored in C–H functionalization,[7] hydride abstraction has been less commonly employed in organic synthesis, aside from intramolecular hydride shifts.[5,8] A few strong Lewis acids have been shown to be potent stoichiometric hydride acceptors, including perfluorinated boranes, trityl cations, and benzoquinones (Scheme 1B).[5,9] In addition, catalytic systems have been developed but are primarily limited to the activation of highly hydridic C–H bonds in electron-rich amines[10] and alcohols.[11]

Recently, progress has been made towards identifying organic hydride acceptors for activating C–H bonds with relatively poor hydricity (i.e., higher $\Delta E_{hydridic}$, more inert C–H bonds). For example, Stahl explored the electrochemical oxidation of carbamates with sub-stoichiometric amounts of unhindered oxoammonium catalysts (Scheme 1C, top).[12] In an ongoing work carried out in our laboratory, we discovered a catalytic variant of this transformation using *m*CPBA as the terminal oxidant, and expanded the reaction scope to the oxidative functionalization of sulfonamides and amides (Scheme 1C, bottom).[13] In this reaction, an inert catalyst-substrate adduct **III** was formed upon hydride transfer, which could be activated to achieve product formation and oxoammonium turnover via a Cope-type elimination in the presence of *m*CPBA.

We envisioned the reactivity of oxoammonium-mediated hydride transfer may be expanded to C–H bonds with even lower hydricity by employing a more potent catalyst. To investigate this hypothesis, we chose to study the oxidation of ethers (Scheme 1D), which are common groups in functional small molecules and polymers.[14] However, their robust chemical stability under a wide range of reaction conditions (e.g., basic, mildly acidic, oxidative, and reductive) limits the utility of ethers as common functional handles in organic synthesis. Historically, the oxidation of ethers to esters relies on the use of strongly oxidizing, high-valent transition metal species such as Cr[15] and Ru[16] oxide complexes, which are often toxic and may limit functional group tolerance. More recently, HAT-based methods have been invented to promote this transformation under milder conditions, but as discussed above, they often display different selectivity profiles vs hydride transfer pathways (Scheme 1B).[7f-h,17] The oxocarbenium ions resulting from hydride abstraction of ethers are versatile synthons and may be further elaborated into myriad functional groups.[18] Therefore, the development of a mild and selective method *via* oxoammonium catalysis may both further enhance the synthetic utility of ether oxidation and advance reaction strategies for C–H functionalization via hydride transfer.

Herein, we present an oxoammonium-catalyzed α-C–H oxidation that converts unactivated ethers to esters via hydride abstraction. An intricate set of equilibria between various catalytic intermediates was identified, which could be modulated using catalytic additives towards optimized oxidation activity. During this study, we also demonstrated NMR relaxometry as a practical tool for in-situ monitoring of organic reactions with radical intermediates.

Scheme 1. Introduction and Background

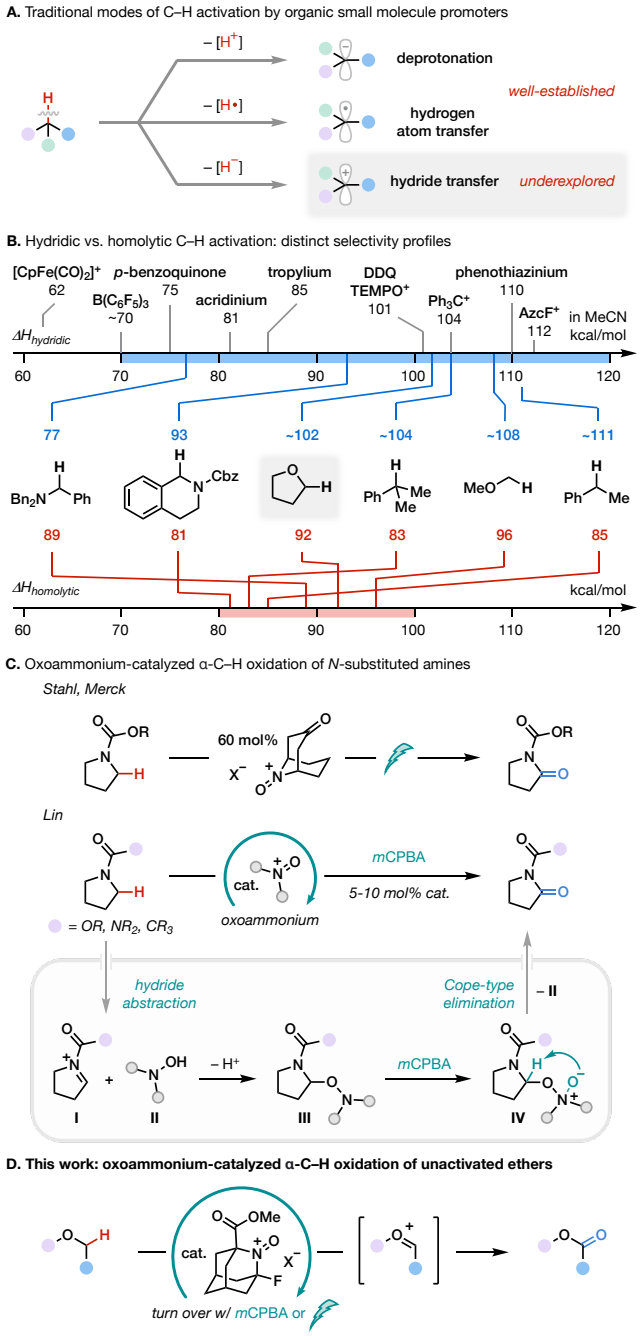

RESULTS AND DISCUSSION

Discovery and Optimization. We began our study with surveying a panel of aminoxyl pre-catalysts for the oxidation of ambroxide (**1**) and observed small quantities of lactone formation in most cases using *m*CPBA as the oxidant in DCM (Table 1, entries 2-6). In addition to known catalysts, we also synthesized a panel of novel aminoxyls including AzcF,[13] a 2-azaadamantane-based molecule with a sterically accessible *N*-oxyl unit. AzcF also exhibits the highest oxidizing potential among the series that we investigated. Indeed, AzcF provided the most promising result, giving desired sclareolide (**2**) in modest 14% yield in 16 h and improved 58% yield after an extended 90 h. We attributed the sluggish reactivity to the presence of 3-chlorobenzoate (*m*CBA, a byproduct derived from *m*CPBA), a coordinating counter anion that inhibits the catalytic oxoammonium ion. To address this issue, we introduced tetrakis(3,5-bis(trifluoromethyl)phenyl)urea, a dual hydrogen-bond donor known to strongly bind benzoate, and observed a four-fold yield improvement (entry 7).[19] In addition, alkali metal salts bearing weakly coordinating anions were effective additives, which presumably freed the oxoammonium via salt metathesis (see Table S3 for details).[20] In particular, 20 mol% $NaSbF_6$ promoted the reaction to achieve 94% yield (entry 8). Lastly, we explored acid additives to sequester benzoate by protonation (entries 9–11) and found that strong protic acids such as TFA (4 equiv) and $HNTf_2$ (5 mol%) led to substantially improved reaction yield. Interestingly, an excessive amount of $HNTf_2$ (20 mol% or more) proved to be detrimental to the reaction (48% yield, Table S2; see discussion below). Oxidation of **1** was demonstrated to be efficient with as low as 1 mol% AzcF catalyst employing $NaSbF_6$ or $HNTf_2$ as additives (entries 14, 15). Finally, alternative oxidants such as magnesium monoperoxyphthalate (MMPP), trichloroisocyanuric acid (TCCA), and ceric ammonium nitrate (CAN) also promoted the oxidation of **1** but were found to display poorer substrate generality than *m*CPBA (entry 16, Table S8 and Table S9).

Table 1. Reaction Discovery

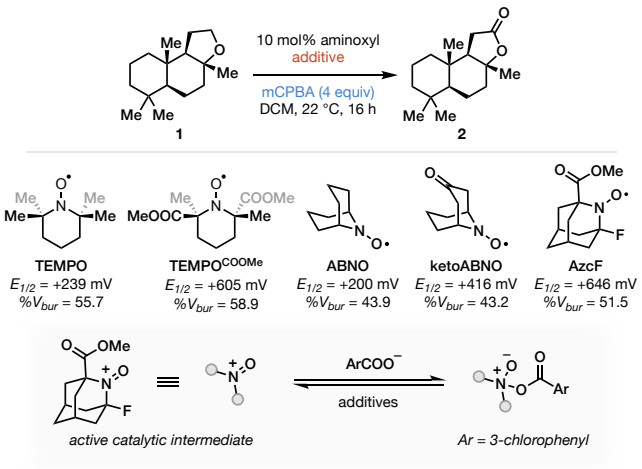

Entry	Conditions[a]	Yield[b] (%)
1	no catalyst	4
2	TEMPO	10 (10)[c]
3	$TEMPO^{COOMe}$	8
4	ABNO	5
5	ketoABNO	5 (5)[c]
6	AzcF	14 (58)[c]
7[d]	AzcF/$urea^{Ar}$	56
8[e]	AzcF/$NaSbF_6$	94
9[f]	AzcF/AcOH	11
10[f]	AzcF/TFA	84
11[g]	**AzcF/$HNTf_2$**	**98**
12[g]	TEMPO/$HNTf_2$	8
13[g]	ketoABNO/$HNTf_2$	64
14[e,h]	AzcF/$NaSbF_6$	95
15[h,i]	AzcF/$HNTf_2$	98

16[i]	AzcF/MMPP, TCCA, CAN	82-90	

[a]All potentials vs. Fc^+/Fc; all buried volumes ($\%V_{bur}$) were calculated for the oxoammoniums of the corresponding aminoxys at 3.0 Å radius;[13] [b]determined by GC; [c]time = 90 h; [d]10 mol% tetrakis(3,5-bis(trifluoromethyl)phenyl)urea; [e]20 mol% additive; [f]4 equiv additive; [g]5 mol% additive; [h]1 mol% aminoxyl, time = 20 h; [i]0.5 mol% additive; [j]conditions in supporting information.

Reactivity and Scope. Under the optimal conditions (Table 1, entry 11), a suite of cyclic ethers with different ring sizes were converted to the corresponding lactones (**3–20**, Figure 2). Arenes with various electron-donating and electron-withdrawing groups (**3**) were compatible with the corresponding desired products formed in high yields. Electronically deactivated alkenes such as acrylate (**4-H**) and cinnamate (**4-Ph**) were tolerated without the observation of competing epoxidation. For substrates that bear benzylic C–H bonds (**5**), we found ether oxidation to be the predominant pathway with minor quantities of dual oxidation products at both α-ether and benzylic sites (products arising from only benzylic oxidation were not formed). Additional functional groups including electron-rich heteroarenes (**6**, **7**; prone to π-oxidation), alkyl halides (**8-Cl, 8-Br**), amide (**8-NHTFA**), esters (**9**, **12**), epoxide (**11**), and cyclopropane (**12**) proved to be compatible. In particular, radical-mediated cyclopropane ring opening was not observed, supporting the proposed hydride transfer mechanism rather than consecutive HAT–oxidation for C–H activation. Indeed, using a radical-based method that was previously reported for the oxidation of THF to γ-butyrolactone,[7h] we did not observe any desired product **12**.

For substrates that are sensitive to strong acids, using $NaSbF_6$ as an additive instead of $HNTf_2$ suppressed undesired side reactions and furnished the products in higher yields, such as **10** (prone to desilylation), **17** (prone to Baeyer-Villiger oxidation), and **18** (prone to hydrolysis). In addition to tetrahydrofurans and tetrahydropyrans, oxetane (**19**) and oxepane (**20**) were also oxidzed to afford *β*- and *ε*-lactones in moderate yield with competing lactone ring opening observed. Finally, we applied this method in the functionalization of synthetic precursors of pharmaceuticals, obtaining lactones **21** (from darunavir intermediate) and **22** (from a fragment of terazosin) in synthetically useful yields.

Scheme 2. Scope of Ether *α*-C–H Oxidation

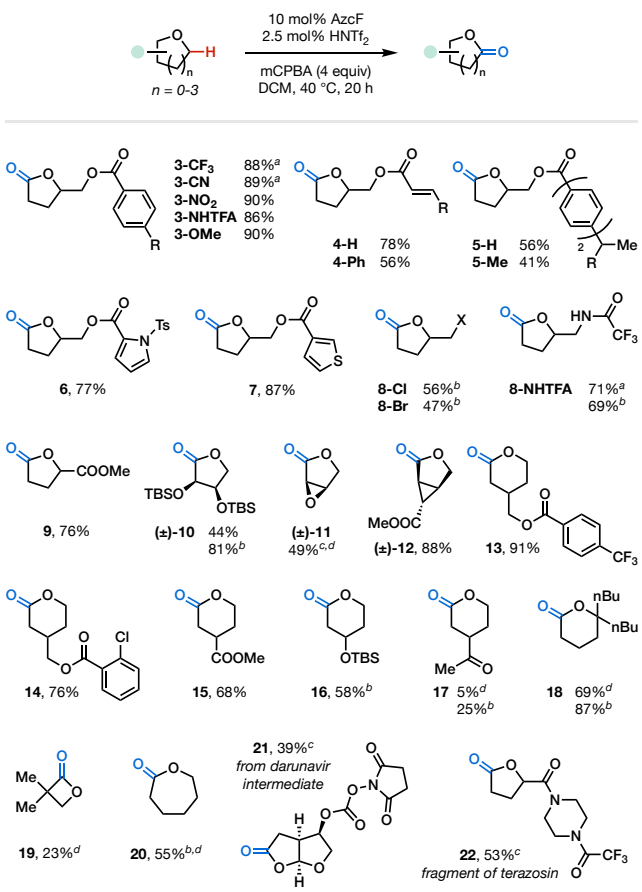

[a]5 mol% AzcF; [b]20 mol% $NaSbF_6$ instead of $HNTf_2$; [c]time = 64 h; [d]Yield determined by ^1H NMR.

During scope exploration, we also observed dearylative oxidation when α-arylethers were subjected to the optimal C–H functionalization conditions (Scheme 3A). For instance, 2-phenyltetrahydrofuran was transformed into γ-butyrolactone **23** in 41% yield without forming any appreciable amount of α-ether oxidation products. We posit that a quinone methide type intermediate was formed following abstraction of the doubly activated C–H bond, as benzoquinone was observed as a byproduct (Scheme 3A, bottom). Under a similar mechanism, natural product sesamin underwent the same transformation to afford pluviatide (**24**) in 39% yield.

Scheme 3. Diverse Transformations from Ether Oxidation

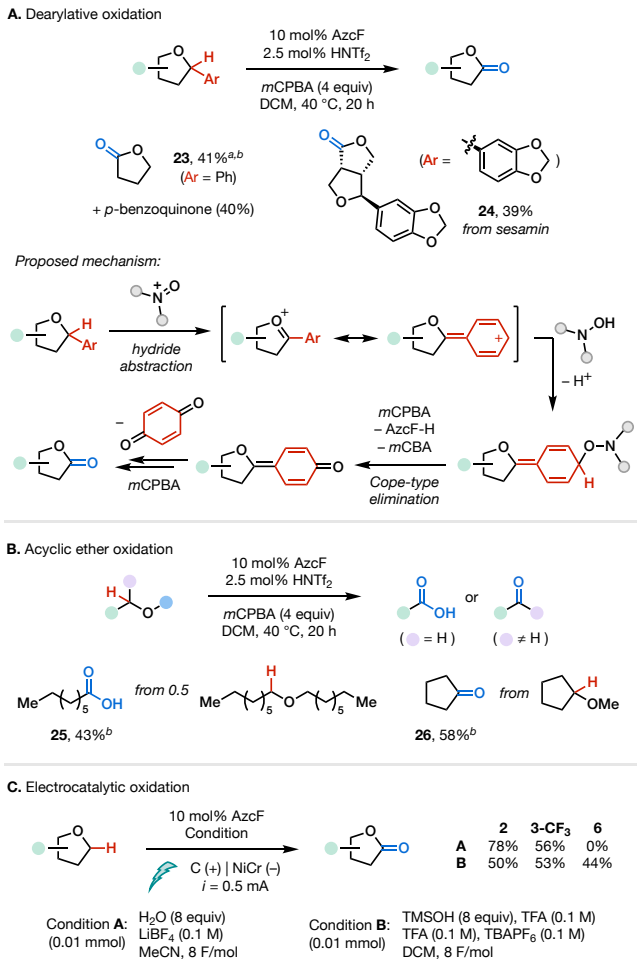

[a]20 mol% $NaSbF_6$ instead of $HNTf_2$; [b]Yield determined by ^1H NMR.

Acyclic ethers were also suitable substrates for AzcF-catalyzed oxidation but chain fragmentation was observed (Scheme 3B). Primary and secondary ethers were converted to the corresponding carboxylic acids and ketones, respectively (**25**, **26**). This reaction could potentially be used for the modification or degradation of ether-containing polymers.

To eliminate the use of a traditional stoichiometric oxidant, we investigated the possibility of an electrocatalytic variant, which was encouraged by promising reactivity observed with single-electron oxidant CAN (Table 1, entry 16). Using 10 mol% AzcF, we identified two sets of electrolysis conditions (Scheme 3C). In Condition A, water was used both as a nucleophile for the desired anodic reaction but also as a sacrificial oxidant for the cathodic hydrogen evolution reaction. Anhydrous conditions (Condition B) were also developed employing trimethylsilanol as a water alternative. These systems show complementary reactivity for a set of three substrates, giving products **2**, **3-CF$_3$**, and **6** in good yield.

Proposed Mechanism. Based on knowledge gained from prior literature and our own experimental findings, we proposed a plausible catalytic cycle for the model reaction using *m*CPBA as the oxidant and $HNTf_2$ as a catalytic additive (Scheme 4). AzcF pre-catalyst (**VI**) was first converted to the active oxoammonium **VIII** to enter the catalytic cycle. Hydride transfer from ambroxide **1** to **VIII** led to the formation of highly electrophilic oxocarbenium intermediate **V** along with hydroxylamine **II**. Rebound of **V** and **II** followed by deprotonation gave rise to aminoacetal **XI**. This substrate-catalyst adduct then underwent further oxidation by *m*CPBA to form tetrahedral *N*-oxide intermediate **XII**, which then decomposed via Cope-type elimination to furnish the desired lactone **2** and hydroxylamine **II**. Finally, oxoammonium **VIII** was regenerated from hydroxylamine **II** and a second equivalent of *m*CPBA to close the cycle. We then carried out a series of experiments to gain further insights into the reaction mechanism. In particular, we aimed to understand the mechanism of formation of oxoammonium **VIII** from either the aminoxyl pre-catalyst (initiation step) or hydroxylamine **II** (turnover step), as well as the mechanism of product formation from aminoacetal **XI**.

Scheme 4. Proposed Mechanism

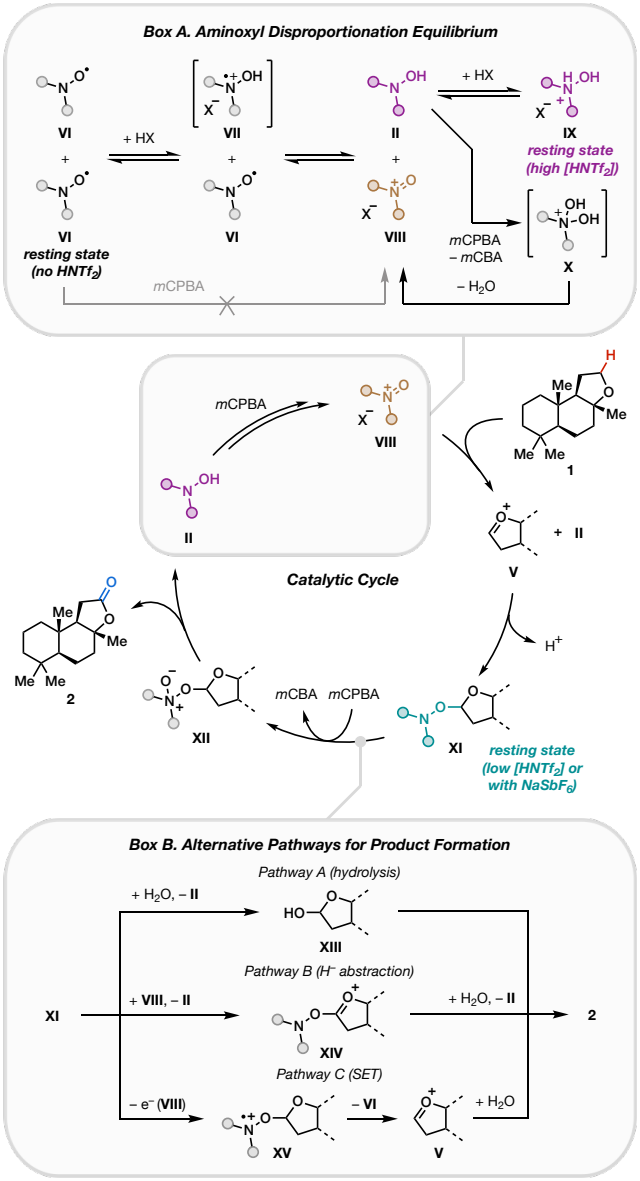

Mechanistic Investigation of Catalytic Turnover. The yield enhancement by shifting the oxoammonium-benzoate association equilibrium is indicative of the presence of multiple

possible catalyst resting states, depending on reaction conditions. This observation prompted us to elucidate and quantify catalytic intermediates during the reaction course. We first performed in-situ UV-vis analysis (Scheme 5A) and found that reaction without an additive (Table 1, entry 6) exhibited spectroscopic features closely matching AzcF radical with an absorbance peak observed at 470 nm. The introduction of $HNTf_2$, however, significantly attenuated this peak. Aminoxyls such as TEMPO are known to undergo disproportionation under acidic conditions.[11a,b] This equilibrium depends on the oxidation potential of the aminoxyl and the acidity of the medium, and has been found to be relevant in oxidative turnover in some catalytic systems.[21] We hypothesize that AzcF shows similar activities. In this case, **VI** would be protonated and then oxidize another equivalent of **VI** to form the corresponding hydroxylamine (**II**) and oxoammonium (**VIII**) (Scheme 4, Box A). The weak basicity of **VI** (vs. TEMPO) and the strongly oxidizing ability of the corresponding oxoammonium ion both favor the comproportionation, making **VI** the resting state under neutral conditions. However, in the catalytic reaction, the low hydricity of ethers necessitates a relatively high concentration of the oxoammonium ion for hydride transfer to take place. Thus, we posit that the addition of super acid $HNTf_2$ plays two roles in enhancing the reactivity of the catalyst; in addition to providing a weakly coordinating counter anion as previously hypothesized, it also aids in shifting the disproportionation equilibrium towards the catalytically active oxoammonium.

To further probe the disproportionation equilibrium of AzcF and understand how it affects the ether oxidation, we carried out reaction monitoring using NMR. ^{1}H NMR is commonly employed to quantify closed-shell species in the kinetic analysis of organic reactions. Direct quantification of open-shell species via ^{1}H NMR suffers from limited signal-to-concentration linearity due to fast relaxation. The Evans method is a state-of-the-art NMR technique for interrogating paramagnetic species and can be used for quantification. In this method, the analyte concentration was calculated from the ^{1}H NMR chemical shift of a reference compound. This renders it unfit for progress monitoring of reaction systems with dynamic chemical environment, as chemical shifts are influenced by factors irrelevant to paramagnetism, such as acidity, solvation effect, and the concentration of the reference compound. While electron paramagnetic resonance (EPR) spectroscopy can be used to identify and quantify open-shell species,[22] it cannot detect closed-shell intermediates simultaneously and is thus inapplicable to wholistic reaction progress analysis.

Indirect quantification approach via paramagnetic relaxation NMR has been established as a practical analytical method. While its main application focuses on applying open-shell species as relaxation enhancing agents for diamagnetic analytes,[23] paramagnetic analytes can also be quantified in reverse with a diamagnetic referencing standard.[24] For instance, Dupree *et al.* have demonstrated the linear relationship between the concentration of 4-hydroxy-TEMPO and the reciprocal of longitudinal relaxation time (T_1) of water, the solvent in this study.[25] We anticipated that a quantification method based on transverse relaxation time (T_2) would share a similar relationship while operationally better-suited for *in situ* reaction monitoring due to the shorter measurement time. To validate this method, spectroscopic titration was performed on TEMPO with 1,1,2,2-tetrachloroethane (TCE) as the diamagnetic reference, exhibiting a linear correlation between concentration of TEMPO and $1/T_2$ of TCE. The same was also found for AzcF within catalytically relevant concentration range, providing a calibration curve for the quantification of AzcF (Scheme 5B).[26] As a proof of concept, we titrated a solution of AzcF with three Brønsted acids with varying acidity and were able to quantitatively assess the disproportionation equilibrium by following the decrease of AzcF. While weak AcOH was ineffective in promoting the disproportionation, both $HNTf_2$ and TFA triggered the recovery of T_2 with the former being particularly efficient (Scheme 5C). Upon addition of 2 equiv of this super acid, we attained complete conversion of AzcF to its oxoammonium form **VIII** and hydroxylammonium **IX**. This trend is consistent with the observed disparate ability of these three acids to facilitate the ether oxidation reaction (Table 1, entries 9-11).

Scheme 5. *In Situ* Observation and Quantification of Catalytic Intermediates

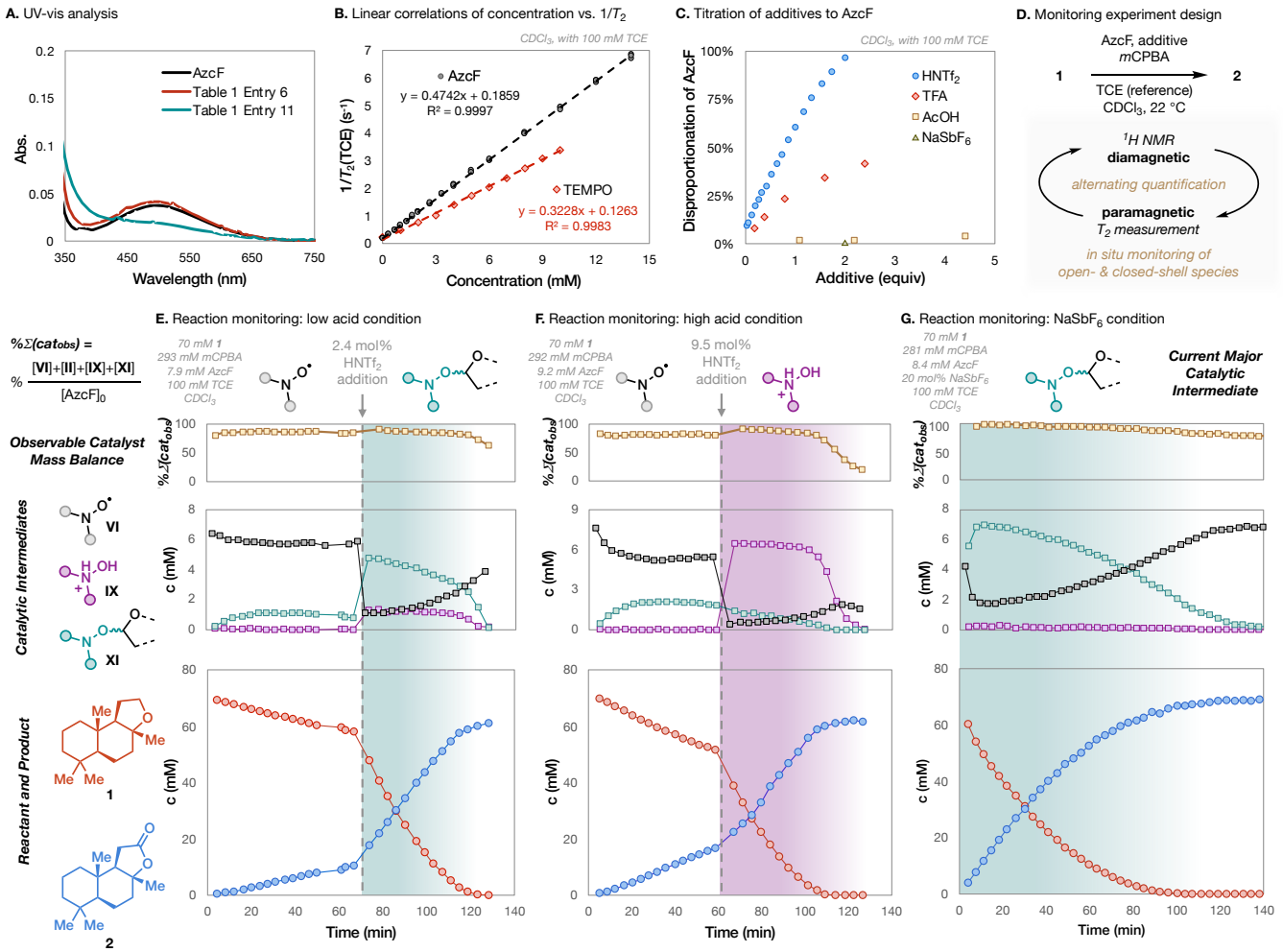

We then employed this NMR relaxometry method in conjunction with standard ^{1}H NMR spectroscopy to determine the catalyst resting states. Through alternatingly performing T_2 measurement and ^{1}H acquisition, both closed-shell and persistent radical species including reactants, products, and catalytically relevant intermediates could be quantitatively observed in real time, and reaction progress could be monitored uninterruptedly in a single NMR experiment (Scheme 5D). $CDCl_3$ was chosen as the solvent for its relatively low vapor pressure and favorable accessibility, and it was shown to be a viable solvent for the model reaction (87% yield under otherwise same conditions as Table 1, entry 11).

We began the experiment under conditions without an acid additive (Scheme 5E-F, left). Using the approach described above, catalytic intermediates including aminoxyl radical **VI** and aminoacetal **XI** were quantified. Hydroxylamine **II** and hydroxylammonium **IX** were observed as a single set of resonances due to rapid proton exchange. Oxoammonium **VIII** was not observable but only accounted for minimal mass balance until upon depletion of **1** at the end of the experiment. The reaction was found to be highly sensitive to traces of strong acids, as DCl from the decomposition of $CDCl_3$ within minutes during sample preparation led to an observable decrease of the concentration of aminoxyl radical **VI**. This promoted the ether oxidation at a slow rate. Nonetheless, the majority of the catalyst stayed as **VI** in the absent of an additive due to the unfavored disproportionation equilibrium.

The addition of catalytic quantities of $HNTf_2$ immediately turned on the ether oxidation reaction. In the presence of a low loading (2.4 mol%) of $HNTf_2$, radical **VI** was first rapidly consumed and then began to slowly build back up as the reaction continued to proceed (black trace, Scheme 5E, right). Aminoacetal **XI** emerged as the predominant form of the catalyst (green trace). A small amount of protonated hydroxylammonium **IX** was also observed. Thus, the resting state of the catalyst in this case was the in-cycle species **XI**. Under these conditions, substrate **1** was efficiently consumed and product **2** formed within *ca.* 50 min.

Interestingly, a higher loading of $HNTf_2$ (9.5 mol%) changed the catalyst resting state (Scheme 5F, right). The rapid disproportionation of **VI** was again observed as evidenced by the immediate consumption of **VI** and formation of hydroxylammonium **IX** as the predominant form of the catalyst, yielding a high concentration of this off-cycle resting state. In contrary to conditions with a low acid loading, we did not observe the accumulation of substrate-catalyst adduct **XI**, and the small amount of **XI** formed due to solvent decomposition into DCl was gradually depleted. Despite the change of catalyst resting

state, the reactivity of ether oxidation was not affected, as the rate of conversion increased significantly upon addition of $HNTf_2$ and reached completion within 50 min (Scheme 5F, right). The change of catalyst resting state to an off-cycle species, however, explains why in the presence of further increased $HNTf_2$ loading (20 mol%), the reaction rate was hampered with decreased yield (48%, Table S2). An increasing proportion of catalyst was unaccounted for as the reaction progressed, which was attributed to the accumulation of oxoammonium **VIII** as supported by the appearance of its characteristic yellow color.

The reaction was also monitored in the presence of 20 mol% $NaSbF_6$ as an additive, which was slower than with $HNTf_2$ but substantially faster than without an additive (Scheme 5G). Adduct **XI** was the dominant aminoxyl species until the end the reaction (>95% conversion). The concentration of **IX** remained insignificant throughout the reaction course. Ex-situ titration experiments showed that $NaSbF_6$ did not significantly alter the direction of the AzcF disproportionation equilibrium (Scheme 5C). As we originally posited, this salt likely promoted the reaction by introducing a non-coordinating anion to render the oxoammonium (**VIII**) more available for hydride abstraction. The mechanism of activation by $NaSbF_6$ and other effective additives in oxoammonium catalysis is a subject of ongoing investigation.

Preparation and Reactivity Study of Catalytic Intermediates. We noted that under all three conditions studied above, at the end of the reaction upon substrate depletion, a significant proportion of the catalyst was present as aminoxyl radical **VI** instead of being fully converted to oxoammonium **VIII**, despite the presence of excessive oxidant *m*CPBA. To further investigate the mechanism of catalytic turnover, an authentic sample of hydroxylamine AzcF-H (**II**) was synthesized *via* hydrogenation of AzcF (**I**) (Scheme 6A). Oxidation of **II** with excess *m*CPBA gave radical **VI** in high yield (Scheme 6B). This transformation is hypothesized to undergo first O-atom transfer from *m*CPBA to **II** followed by elimination of OH^- to furnish oxoammonium **VIII**, which then reacted with hydroxylamine **II** *via* comproportionating to afford radical **VI** (Scheme 4, Box A). Thus, *m*CPBA—typically considered as a two-electron oxidant and O-atom donor—can readily oxidize hydroxylamine **II** yet cannot effect the one-electron oxidation of aminoxyl **VI**.[27] This characteristic necessitates the use of a strong acid to turn over the catalyst and regenerate the active oxoammonium ion by promoting aminoxyl disproportionation. On the contrary, when a strong one-electron oxidant $NOSbF_6$ (+870 mV vs. Fc^+/Fc) was used, AzcF **VI** was oxidized to **VIII**, a benchtop stable crystalline solid, in 79% yield (Scheme 6C).

We also found that aminoacetal **XI** could be synthesized independently by reacting ambroxide **1** with **VIII**, which was isolated as a mixture with **1** and sclareolide **2**. Attempts to obtain pure **27** failed as it decomposed into **2** during purification. We hypothesize that four pathways could account for the conversion of **XI** to product **2** in the model catalytic reaction, all of which could contribute to the observed reactivity (Scheme 4, box B). In addition to the originally hypothesized Cope-type elimination process promoted by *m*CPBA, **XI** could also undergo acid-promoted hydrolysis (the reaction generated H_2O as a byproduct) followed by oxidation of the resultant hemiacetal (**XIII**), or alternatively a second hydride transfer from adduct **XI** to oxoammonium **VIII** followed by hydrolysis and further oxidation.[28] Finally, a single-electron oxidation of **XI** by oxoammonium **VIII** would generate radical cation **XV**, which would undergo mesolytic cleavage[29] to form oxocarbenium **V** followed by water trapping and subsequent oxidation to the lactone.

The poor hydrolytic stability of **XI** we observed during its isolation supports the possibility of alternative pathway A. In support of alternative pathways B and C, we subjected ether **1** to **VIII**, either directly added as a reagent or generated in situ from acid-promoted disproportionation of AzcF, and observed formation of product **2** (Scheme 6E). These results showed that the presence of *m*CPBA or $HNTf_2$, while important for catalytic turnover, was not strictly necessary for the decomposition of intermediate **XI** into product **2**. However, *m*CPBA was the most effective oxidant for the oxidation of a broad range of substrates and the only one that provided satisfactory catalytic turnover for challenging tetrahydropyran-type substrates (see Tables S8, S9 and Scheme S1), which lends support to the proposed Cope-elimination mechanism being the predominant pathway for product formation.

Scheme 6. Syntheses and Reactivity Study of Catalytic Intermediates

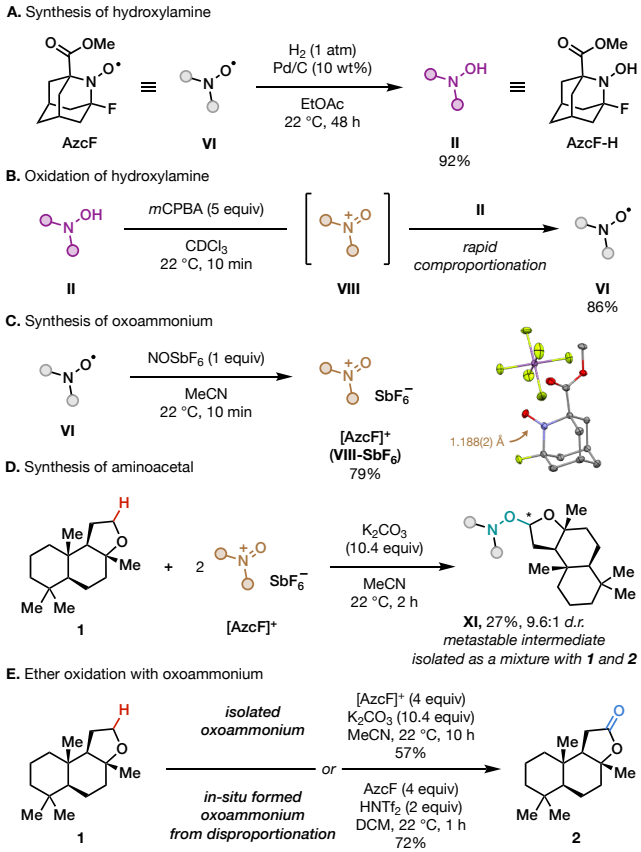

CONCLUSION

In conclusion, we developed an oxoammonium-catalyzed oxidation of ethers to lactones via a hydride abstraction mechanism. The disproportionation equilibrium of the aminoxyl catalyst precursor, which could be tuned using catalytic acid or salt additives, alters the resting state of the catalyst and strongly influences the reactivity. We employed paramagnetic relaxation enhancement NMR to quantify the aminoxyl radical, which enabled in situ monitoring of various catalytic intermediates when used together with standard ^1H NMR acquisition. Ongoing

efforts are directed towards furthering understanding and applying oxoammonium catalysis in the functionalization of other types of C–H bonds via hydride transfer.

AUTHOR INFORMATION

Corresponding Author

Song Lin − *Department of Chemistry and Chemical Biology, Cornell University, Ithaca, New York 14853, United States;* orcid.org/0000-0002-8880-6476; Email: songlin@cornell.edu

Authors

Yukun Cheng − *Department of Chemistry and Chemical Biology, Cornell University, Ithaca, New York 14853, United States;* orcid.org/0000-0002-2379-9404

Jonas Rein − *Department of Chemistry and Chemical Biology, Cornell University, Ithaca, New York 14853, United States;* orcid.org/0000-0001-8237-6519

Nguyen Le − *Department of Chemistry and Chemical Biology, Cornell University, Ithaca, New York 14853, United States;* orcid.org/0009-0009-2009-479X

ACKNOWLEDGMENT

Research was supported by the NIH (R01GM134088). S.L. is grateful to Bristol Myers Squibb for an Unrestricted Grant in Synthetic Organic Chemistry. We thank Dr. Samantha N. MacMillan (Cornell University) for collection of X-ray crystallographic data; Dr. Ivan Keresztes (Cornell University) for helpful discussion on NMR experiments; Dr. Yi Wang (Cornell University) for helpful discussion on computational experiments; Dr. James E. McGettigan Jr. (Cornell University) for reproducing experiments; and Tianwei Chen (Cornell University) for experimental assistance.

REFERENCES

(1) For representative reviews see: (a) Davies, H. M. L.; Du Bois, J.; Yu, J.-Q. C–H Functionalization in Organic Synthesis. *Chem. Soc. Rev.* **2011**, *40* (4), 1855–1856. (b) Gutekunst, W. R.; Baran, P. S. C–H Functionalization Logic in Total Synthesis. *Chem. Soc. Rev.* **2011**, *40* (4), 1976–1991. (c) Wencel-Delord, J.; Glorius, F. C–H Bond Activation Enables the Rapid Construction and Late-Stage Diversification of Functional Molecules. *Nat. Chem.* **2013**, *5* (5), 369–375. (d) Cernak, T.; Dykstra, K. D.; Tyagarajan, S.; Vachal, P.; Krska, S. W. The Medicinal Chemist's Toolbox for Late Stage Functionalization of Drug-like Molecules. *Chem. Soc. Rev.* **2016**, *45* (3), 546–576. (e) Dalton, T.; Faber, T.; Glorius, F. C–H Activation: Toward Sustainability and Applications. *ACS Cent. Sci.* **2021**, *7* (2), 245–261.

(2) For representative reviews, see: (a) Rogge, T.; Kaplaneris, N.; Chatani, N.; Kim, J.; Chang, S.; Punji, B.; Schafer, L. L.; Musaev, D. G.; Wencel-Delord, J.; Roberts, C. A; Sarpong, R.; Wilson, Z. E.; Brimble, M. A.; Johansson, M. J.; Ackermann, L. C–H Activation. *Nat. Rev. Methods Primers* **2021**, *1* (1), 43. (b) He, J.; Wasa, M.; Chan, K. S. L.; Shao, Q.; Yu, J.-Q. Palladium-Catalyzed Transformations of Alkyl C–H Bonds. *Chem. Rev.* **2017**, *117* (13), 8754–8786. (c) Li, J.; De Sarkar, S.; Ackermann, L. Meta- and Para-Selective C–H Functionalization by C–H Activation. In *C-H Bond Activation and Catalytic Functionalization I. Topics in Organometallic Chemistry*; Dixneuf, P., Doucet, H., Eds.; Springer, 2015; pp 217–257. (d) Costas, M. Selective C–H Oxidation Catalyzed by Metalloporphyrins. *Coord. Chem. Rev.* **2011**, *255* (23-24), 2912–2932. (e) White, M. C.; Zhao, J. Aliphatic C–H Oxidations for Late-Stage Functionalization. *J. Am. Chem. Soc.* **2018**, *140* (43), 13988–14009. (f) Zhang, Z.; Chen, P.; Liu, G. Copper-Catalyzed Radical Relay in C(sp^3)–H Functionalization. *Chem. Soc. Rev.* **2022**, *51* (5), 1640–1658.

(3) For representative reviews and examples, see: (a) Soltani, Y.; Fontaine, F.-G. FLP-Mediated C–H-Activation. In *Frustrated Lewis Pairs. Molecular Catalysis*; Slootweg, C. J., Jupp, A. R., Eds.; Springer, 2021; pp 113–166. (b) Qin, Y.; Zhu, L.; Luo, S. Organocatalysis in Inert C–H Bond Functionalization. *Chem. Rev.* **2017**, *117* (13), 9433–9520. (c) Campos, K. R.; Klapars, A.; Waldman, J. H.; Dormer, P. G.; Chen, C. Enantioselective, Palladium-Catalyzed α-Arylation of N-Boc-Pyrrolidine. *J. Am. Chem. Soc.* **2006**, *128* (11), 3538–3539. (d) Campos, K. R. Direct sp^3 C–H Bond Activation Adjacent to Nitrogen in Heterocycles. *Chem. Soc. Rev.* **2007**, *36* (7), 1069–1084. (e) Grant, P. S.; Vavrík, M.; Porte, V.; Meyrelles, R.; Maulide, N. Remote Proton Elimination: C–H Activation Enabled by Distal Acidification. *Science* **2024**, *384* (6697), 815–820. (f) Li, C.-J. Cross-Dehydrogenative Coupling (CDC): Exploring C−C Bond Formations beyond Functional Group Transformations. *Acc. Chem. Res.* **2008**, *42* (2), 335–344.

(4) For representative reviews, see: (a) Golden, D. L.; Suh, S.-E.; Stahl, S. S. Radical C(sp^3)–H Functionalization and Cross-Coupling Reactions. *Nat. Rev. Chem.* **2022**, *6* (6), 405–427. (b) Capaldo, L.; Ravelli, D.; Fagnoni, M. Direct Photocatalyzed Hydrogen Atom Transfer (HAT) for Aliphatic C–H Bonds Elaboration. *Chem. Rev.* **2022**, *122* (2), 1875–1924. (c) Galeotti, M.; Salamone, M.; Bietti, M. Electronic Control over Site-Selectivity in Hydrogen Atom Transfer (HAT) Based C(sp^3)–H Functionalization Promoted by Electrophilic Reagents. *Chem. Soc. Rev.* **2022**, *51* (6), 2171–2223. (d) Ruffoni, A.; Mykura, R. C.; Bietti, M.; Leonori, D. The Interplay of Polar Effects in Controlling the Selectivity of Radical Reactions. *Nat. Synth.* **2022**, *1* (9), 682–695.

(5) For representative reviews, see: (a) Liu, L. Hydride-Abstraction-Initiated Catalytic Stereoselective Intermolecular Bond-Forming Processes. *Acc. Chem. Res.* **2022**, *55* (23), 3537–3550. (b) Miller, J. L.; Lawrence, J.-M. I. A.; Rodriguez del Rey, F. O.; Floreancig, P. E. Rodriguez del Rey, F. O.; Floreancig, P. E. Synthetic Applications of Hydride Abstraction Reactions by Organic Oxidants. *Chem. Soc. Rev.* **2022**, *51* (13), 5660–5690.

(6) Luo, W.; Yang, J.-D.; Cheng, J.-P. Toward Rational Understandings of α-C–H Functionalization: Energetic Studies of Representative Tertiary Amines. *iScience* **2020**, *23* (2), 100851.

(7) For examples, see: (a) Stateman, L. M.; Nakafuku, K. M.; Nagib, D. A. Remote C–H Functionalization via Selective Hydrogen Atom Transfer. *Synthesis* **2018**, *50* (08), 1569–1586. (b) Fazekas, T. J.; Alty, J. W.; Neidhart, E. K.; Miller, A. S.; Leibfarth, F. A.; Alexanian, E. J. Diversification of Aliphatic C–H Bonds in Small Molecules and Polyolefins through Radical Chain Transfer. *Science* **2022**, *375* (6580), 545–550. (c) Horn, E. J.; Rosen, B. R.; Chen, Y.; Tang, J.; Chen, K.; Eastgate, M. D.; Baran, P. S. Scalable and Sustainable Electrochemical Allylic C–H Oxidation. *Nature* **2016**, *533* (7601), 77–81. (d) Shu, C.; Noble, A.; Aggarwal, V. K. Metal-Free Photoinduced C(sp^3)–H Borylation of Alkanes. *Nature* **2020**, *586* (7831), 714–719. (e) Davies, J.; Morcillo, S. P.; Douglas, J. J.; Leonori, D. Hydroxylamine Derivatives as Nitrogen-Radical Precursors in Visible-Light Photochemistry. *Chem. Eur. J.* **2018**, *24* (47), 12154–12163. (f) Pierce, C. J.; Hilinski, M. K. Chemoselective Hydroxylation of Aliphatic sp^3 C–H Bonds Using a Ketone Catalyst and Aqueous H_2O_2. *Org. Lett.* **2014**, *16* (24), 6504–6507. (g) Lu, Z.-P.; Ju, M.; Wang, Y.; Meinhardt, J. M.; Martinez, J. I.; Villemure, E.; Terrett, J. A.; Lin, S. Regioselective Aliphatic C–H Functionalization Using Frustrated Radical Pairs. *Nature* **2023**, *619* (7970), 514–520. (h) Zhao, Y.; Ang, J. Q. L.; Ng, A. W. T.; Yeung, Y.-Y. Oxidative Transformation of Cyclic Ethers/Amines to Lactones/Lactams Using a DIB/TBHP Protocol. *RSC Adv.* **2013**, *3* (43), 19765–19768. (i) Zhang, Y.; Fitzpatrick, N. A.; Das, M.; Bedre, I. P.; Yayla, H. G.; Lall, M. S.; Musacchio, P. Z. A Photoredox-Catalyzed Approach for Formal Hydride Abstraction to Enable C –H Functionalization with Nucleophilic Partners (F, C, O, N, and Br/Cl). *Chem Catal.* **2022**, *2* (2), 292–308. (j) Paolillo, J. M.; Duke, A. D.; Gogarnoiu, E. S.; Wise, D. E.; Parasram, M. Anaerobic Hydroxylation of C(sp^3)–H Bonds Enabled by the Synergistic Nature of Photoexcited Nitroarenes. *J. Am. Chem. Soc.* **2023**, *145* (5), 2794–2799.

(8) (a) Kwon, S. J.; Kim, D. Y. Organo- and Organometallic-Catalytic Intramolecular [1,5]-Hydride Transfer/Cyclization Process through C(sp^3)-H Bond Activation. *Chem. Rec.* **2016**, *16* (3), 1191–1203. (b) Shen, Y.-B.; Hu, F.; Li, S.-S. Alkyl Amines and Ethers as Traceless Hydride Donors in [1,5]-Hydride Transfer Cascade Reactions. *Org. Biomol. Chem.* **2023**, *21* (4), 700–714. (c) (e) Murarka, S.; Deb, I.; Zhang, C.; Seidel, D. Catalytic Enantioselective

Intramolecular Redox Reactions: Ring-Fused Tetrahydroquinolines. *J. Am. Chem. Soc.* **2009**, *131* (37), 13226–13227. (f) Haibach, M. C.; Deb, I.; De, C. K.; Seidel, D. Redox-Neutral Indole Annulation Cascades. *J. Am. Chem. Soc.* **2011**, *133* (7), 2100–2103. (h) McQuaid, K. M.; Sames, D. C−H Bond Functionalization via Hydride Transfer: Lewis Acid Catalyzed Alkylation Reactions by Direct Intramolecular Coupling of sp^3 C−H Bonds and Reactive Alkenyl Oxocarbenium Intermediates. *J. Am. Chem. Soc.* **2009**, *131* (2), 402–403. (i) McQuaid, K. M.; Long, J. Z.; Sames, D. C−H Bond Functionalization via Hydride Transfer: Synthesis of Dihydrobenzopyrans from *ortho*-Vinylaryl Akyl Ethers. *Org. Lett.* **2009**, *11* (14), 2972–2975. (j) Vadola, P. A.; Sames, D. C−H Bond Functionalization via Hydride Transfer: Direct Coupling of Unactivated Alkynes and sp^3 C−H Bonds Catalyzed by Platinum Tetraiodide. *J. Am. Chem. Soc.* **2009**, *131* (45), 16525–16528.

(9) (a) Barton, D. H. R.; Magnus, P. D.; Smith, G.; Streckert, G.; Zurr, D. Experiments on the Synthesis of Tetracycline. Part XI. Oxidation of Ketone Acetals and Ethers by Hydride Transfer. *J. Chem. Soc. Perkin Trans. 1* **1972**, 542–552. (b) Gunther, S. O.; Lee, C.-I.; Song, E.; Bhuvanesh, N.; Ozerov, O. V. Isolable Fluorinated Triphenylmethyl Cation Salts of $[HCB_{11}Cl_{11}]^-$: Demonstration of Remarkable Hydride Affinity. *Chem. Sci.* **2022**, *13* (17), 4972–4976. (c) Holthausen, M. H.; Mahdi, T.; Schlepphorst, C.; Hounjet, L. J.; Weigand, J. J.; Stephan, D. W. Frustrated Lewis Pair-Mediated C–O or C–H Bond Activation of Ethers. *Chem. Commun.* **2014**, *50* (70), 10038–10040. (d) Yesilcimen, A.; Jiang, N.-C.; Gottlieb, F. H.; Wasa, M. Enantioselective Organocopper-Catalyzed Hetero Diels–Alder Reaction through in Situ Oxidation of Ethers into Enol Ethers. *J. Am. Chem. Soc.* **2022**, *144* (14), 6173–6179.

(10) (a) Chang, Y.; Cao, M.; Chan, J. Z.; Zhao, C.; Wang, Y.; Yang, R.; Wasa, M. Enantioselective Synthesis of N -Alkylamines through β-Amino C–H Functionalization Promoted by Cooperative Actions of $B(C_6F_5)_3$ and a Chiral Lewis Acid Co-Catalyst. *J. Am. Chem. Soc.* **2021**, *143* (5), 2441–2455. (b) Chang, Y.; Yesilcimen, A.; Cao, M.; Zhang, Y.; Zhang, B.; Chan, J. Z.; Wasa, M. Catalytic Deuterium Incorporation within Metabolically Stable β-Amino C–H Bonds of Drug Molecules. *J. Am. Chem. Soc.* **2019**, *141* (37), 14570–14575. (c) Farrell, J. M.; Heiden, Z. M.; Stephan, D. W. Metal-Free Transfer Hydrogenation Catalysis by $B(C_6F_5)_3$. *Organometallics* **2011**, *30* (17), 4497–4500. (d) Maier, A. F. G.; Tussing, S.; Zhu, H.; Wicker, G.; Tzvetkova, P.; Flörke, U.; Daniliuc, C. G.; Grimme, S.; Paradies, J. Borane-Catalyzed Synthesis of Quinolines Bearing Tetrasubstituted Stereocenters by Hydride Abstraction-Induced Electrocyclization. *Chem. Eur. J.* **2018**, *24* (61), 16287–16291.

(11) (a) Nutting, J. E.; Rafiee, M.; Stahl, S. S. Tetramethylpiperidine *N*-Oxyl (TEMPO), Phthalimide *N*-Oxyl (PINO), and Related *N*-Oxyl Species: Electrochemical Properties and Their Use in Electrocatalytic Reactions. *Chem. Rev.* **2018**, *118* (9), 4834–4885. (b) Leifert, D.; Studer, A. Organic Synthesis Using Nitroxides. *Chem. Rev.* **2023**, *123* (16), 10302–10380. (c) Wang, F.; Stahl, S. S. Electrochemical Oxidation of Organic Molecules at Lower Overpotential: Accessing Broader Functional Group Compatibility with Electron−Proton Transfer Mediators. *Acc. Chem. Res.* **2020**, *53* (3), 561–574. (d) Rein, J.; Rozema, S. D.; Langner, O. C.; Zacate, S. B.; Hardy, M. A.; Siu, J. C.; Mercado, B. Q.; Sigman, M. S.; Miller, S. J.; Lin, S. Generality-Oriented Optimization of Enantioselective Aminoxyl Radical Catalysis. *Science* **2023**, *380* (6646), 706–712.

(12) (a) Wang, F.; Rafiee, M.; Stahl, S. S. Electrochemical Functional-Group-Tolerant Shono-type Oxidation of Cyclic Carbamates Enabled by Aminoxyl Mediators. *Angew. Chem. Int. Ed.* **2018**, *57* (22), 6686–6690. (b) Deprez, N. R.; Clausen, D. J.; Yan, J.-X.; Peng, F.; Zhang, S.; Kong, J.; Bai, Y. Selective Electrochemical Oxidation of Functionalized Pyrrolidines. *Org. Lett.* **2021**, *23* (22), 8834–8837.

(13) Rein, J.; Gorski, B.; Cheng, Y.; Lei, Z.; Buono, F.; Lin, S. Oxoammonium-Catalyzed Oxidation of *N*-Protected Amines. *ChemRxiv* **2024**.

(14) (a) Nakata, T. Total Synthesis of Marine Polycyclic Ethers. *Chem. Rev.* **2005**, *105* (12), 4314–4347. (b) María, P. D. de; van Gemert, R. W.; Straathof, A. J. J.; Hanefeld, U. Biosynthesis of Ethers: Unusual or Common Natural Events? *Nat. Prod. Rep.* **2010**, *27* (3), 370–392. (c) Tang, S.; Baker, G. A.; Zhao, H. Ether- and Alcohol-Functionalized Task-Specific Ionic Liquids: Attractive Properties and Applications. *Chem. Soc. Rev.* **2012**, *41* (10), 4030–4066. (d) Fabre, B.; Simonet, J. Electroactive Polymers Containing Crown Ether or Polyether Ligands as Cation-Responsive Materials. *Coord. Chem. Rev.* **1998**, *178-180*, 1211–1250. (e) Sifri, R. J.; Ma, Y.; Fors, B. P. Photoredox Catalysis in Photocontrolled Cationic Polymerizations of Vinyl Ethers. *Acc. Chem. Res.* **2022**, *55* (14), 1960–1971.

(15) For examples of total syntheses that employ high-valent Cr oxide as a catalyst or reagent for ether to ester oxidation, see: (a) Limanto, J.; Snapper, M. L. Sequential Intramolecular Cyclobutadiene Cycloaddition, Ring-Opening Metathesis, and Cope Rearrangement: Total Syntheses of (+)- and (−)-Asteriscanolide. *J. Am. Chem. Soc.* **2000**, *122* (33), 8071–8072. (b) Abelman, M. M.; Overman, L. E.; Tran, V. D. Construction of Quaternary Carbon Centers by Palladium-Catalyzed Intramolecular Alkene Insertions. Total Synthesis of the Amaryllidaceae Alkaloids (.+-.)-Tazettine and (.+-.)-6a-Epipretazettine. *J. Am. Chem. Soc.* **1990**, *112* (19), 6959–6964. (c) Johnson, T. C.; Chin, M. R.; Siegel, D. Synthetic Route Development for the Laboratory Preparation of Eupalinilide E. *J. Org. Chem.* **2017**, *82* (9), 4640–4653. (d) Ruider, S. A.; Carreira, E. M. A Unified Strategy to Plakortin Pentalenes: Total Syntheses of (±)-Gracilioethers E and F. *Org. Lett.* **2015**, *18* (2), 220–223. (e) Zheng, C.; Dubovyk, I.; Lazarski, K. E.; Thomson, R. J. Enantioselective Total Synthesis of (−)-Maoecrystal V. *J. Am. Chem. Soc.* **2014**, *136* (51), 17750–17756.

(16) For examples of total syntheses that employ high-valent Ru oxide as a catalyst or reagent for ether to ester oxidation, see: (a) Yoshimitsu, T.; Makino, T.; Nagaoka, H. Synthesis of (−)-Muricatacin via α- and α'-C−H Bond Functionalization of Tetrahydrofuran. *J. Org. Chem.* **2003**, *68* (19), 7548–7550. (b) Aggarwal, V. K.; Davies, P. W.; Schmidt, A. T. Asymmetric Synthesis of Avenaciolide *via* Cascade Palladium Catalysed Cyclisation–Carbonylation of Bromodienes. *Chem. Commun.* **2004**, *10*, 1232–1233. (c) Burke, S. D.; K. Shankaran; Margaret Jones Helber. Synthesis of (+)-Fragolide and (−)-Pereniporin B via Vinylsilane Terminated Cationic Cyclization. *Tetrahedron Lett.* **1991**, *32* (36), 4655–4658. (d) Fu, J.; Shen, H.; Chang, Y.; Li, C.; Gong, J.; Yang, Z. Concise Stereoselective Synthesis of Oxaspirocycles with 1-Tosyl-1,2,3-Triazoles: Application to the Total Syntheses of (±)-Tuberostemospiroline and (±)-Stemona-Lactam R. *Chem. Eur. J.* **2014**, *20* (40), 12881–12888. (e) Shah, U.; Chackalamannil, S.; Ganguly, A. K.; Chelliah, M.; Kolotuchin, S.; Buevich, A.; McPhail, A. Total Synthesis of (−)-Himgaline. *J. Am. Chem. Soc.* **2006**, *128* (39), 12654–12655.

(17) (a) Chen, M. S.; White, M. C. Combined Effects on Selectivity in Fe-Catalyzed Methylene Oxidation. *Science* **2010**, *327* (5965), 566–571. (b) Clemente-Tejeda, D.; López-Moreno, A.; Bermejo, F. A. Non-heme iron catalysis in C=C, C–H, and CH_2 oxidation reactions. Oxidative transformations on terpenoids catalyzed by $Fe(bpmen)(OTf)_2$. *Tetrahedron* **2013**, *69* (14), 2977–2986. (c) Iqbal, J.; Srivastava, R. R. Cobalt(II) Chloride Catalysed Cleavage of Ethers with Acyl Halides: Scope and Mechanism. *Tetrahedron* **1991**, *47* (18-19), 3155–3170. (d) Dai, Z.-Y.; Zhang, S.-Q.; Hong, X.; Wang, P.-S.; Gong, L.-Z. A Practical $FeCl_3$/HCl Photocatalyst for Versatile Aliphatic C–H Functionalization. *Chem Catal.* **2022**, *2* (5), 1211–1222. (e) Liu, Y.; Nie, B.; Li, N.; Liu, H.; Wang, F. Chlorine Radical-Mediated Photocatalytic C(Sp3)−H Bond Oxidation of Aryl Ethers to Esters. *Chin. J. Catal.* **2024**, *58*, 123–128.

(18) (a) Wan, T.; Capaldo, L.; Laudadio, G.; Nyuchev, A. V.; Rincón, J. A.; García-Losada, P.; Mateos, C.; Frederick, M. O.; Nuño, M.; Noël, T. Decatungstate-Mediated C(sp^3)–H Heteroarylation via Radical-Polar Crossover in Batch and Flow. *Angew. Chem. Int. Ed.* **2021**, *60* (33), 17893–17897. (b) Pulcinella, A.; Bonciolini, S.; Lukas, F.; Sorato, A.; Noël, T. Photocatalytic Alkylation of C(sp^3)−H Bonds Using Sulfonylhydrazones. *Angew. Chem. Int. Ed.* **2023**, *62* (3), No. e202215374. (c) Ioannou, D. I.; Capaldo, L.; Sanramat, J.; Reek, J. N. H.; Noël, T. Accelerated Electrophotocatalytic C(sp^3)−H Heteroarylation Enabled by an Efficient Continuous-Flow Reactor. *Angew. Chem. Int. Ed.* **2023**, *62* (52), No. e202315881.

(19) Klausen, R. S.; Kennedy, C. R.; Hyde, A. M.; Jacobsen, E. N. Chiral Thioureas Promote Enantioselective Pictet–Spengler Cyclization by Stabilizing Every Intermediate and Transition State in

the Carboxylic Acid-Catalyzed Reaction. *J. Am. Chem. Soc.* **2017**, *139* (35), 12299–12309.

(20) (a) Shibuya, M.; Tomizawa, M.; Iwabuchi, Y. Oxidative Rearrangement of Tertiary Allylic Alcohols Employing Oxoammonium Salts. *J. Org. Chem.* **2008**, *73* (12), 4750–4752. (b) Nagasawa, S.; Sasano, Y.; Iwabuchi, Y. Catalytic Oxygenative Allylic Transposition of Alkenes into Enones with an Azaadamantane‐Type Oxoammonium Salt Catalyst. *Chem. Eur. J.* **2017**, *23* (43), 10276–10279. (c) Miller, S. A.; Nandi, J.; Leadbeater, N. E.; Eddy, N. A. Probing the Effect of Counterions on the Oxidation of Alcohols Using Oxoammonium Salts. *Eur. J. Org. Chem.* **2019**, *2020* (1), 108–112.

(21) (a) De Mico, A.; Margarita, R.; Parlanti, L.; Vescovi, A.; Piancatelli, G. A Versatile and Highly Selective Hypervalent Iodine (III)/2,2,6,6-Tetramethyl-1-Piperidinyloxyl-Mediated Oxidation of Alcohols to Carbonyl Compounds. *J. Org. Chem.* **1997**, *62* (20), 6974–6977. (b) Hayashi, M.; Shibuya, M.; Iwabuchi, Y. Oxidation of Alcohols to Carbonyl Compounds with Diisopropyl Azodicarboxylate Catalyzed by Nitroxyl Radicals. *J. Org. Chem.* **2012**, *77* (6), 3005–3009.

(22) (a) Qi, J.-Q.; Suo, W.; Liu, J.; Sun, S.; Jiao, L.; Guo, X. Direct Observation of All Open-Shell Intermediates in a Photocatalytic Cycle. *J. Am. Chem. Soc.* **2024**, *146* (11), 7140–7145. (b) Zhang, S.; Cheng, L.; Qi, J.-Q.; Jia, Z.; Zhang, L.; Jiao, L.; Guo, X.; Luo, S. Characterization and Monitoring of Transient Enamine Radical Intermediates in Photoredox/Chiral Primary Amine Synergistic Catalysis Cycle. *CCS Chem.* **2024**, 1–7.

(23) (a) Carr, T. M.; Ritchey, W. M. Toward an Optimal Paramagnetic Relaxation Agent for ^{31}P NMR Spectroscopy. *Spectrosc. Lett.* **1980**, *13* (9), 603–633. (b) Fischer, H. H.; Seiler, M.; Ertl, T. S.; Eberhardinger, U.; Bertagnolli, H.; Schmitt-Willich, H.; Albert, K. Quantification Studies in Continuous-Flow ^{13}C Nuclear Magnetic Resonance Spectroscopy by Use of Immobilized Paramagnetic Relaxation Agents. *J. Phys. Chem. B* **2003**, *107* (20), 4879–4886. (c) Bara-Estaún, A.; Harder, M. C.; Lyall, C. L.; Lowe, J. P.; Suturina, E.; Hintermair, U. Paramagnetic Relaxation Agents for Enhancing Temporal Resolution and Sensitivity in Multinuclear FlowNMR Spectroscopy. *Chem. Eur. J.* **2023**, *29* (38), No. e202300215.

(24) (a) D'Agostino, C.; Bräuer, P.; Charoen-Rajapark, P.; Crouch, M. D.; Gladden, L. F. Effect of Paramagnetic Species on T_1, T_2 and T_1/T_2 NMR Relaxation Times of Liquids in Porous $CuSO_4/Al_2O_3$. *RSC Adv.* **2017**, *7* (57), 36163–36167. (b) Gomes, B. F.; Burato, J. S. da S.; Silva Lobo, C. M.; Colnago, L. A. Use of the Relaxometry Technique for Quantification of Paramagnetic Ions in Aqueous Solutions and a Comparison with Other Analytical Methods. *Int. J. Anal. Chem.* **2016**, *2016*, 1–5.

(25) Kryukov, E. V.; Pike, K. J.; Tam, T. K. Y.; Newton, M. E.; Smith, M. E.; Dupree, R. Determination of the Temperature Dependence of the Dynamic Nuclear Polarisation Enhancement of Water Protons at 3.4 Tesla. *Phys. Chem. Chem. Phys.* **2011**, *13* (10), 4372–4380.

(26) We note the T_2 measurement was performed under ambient atmosphere, which is consistent with the synthetic conditions developed for ether oxidation. Under such conditions, O_2 also contributes to the relaxation enhancement but does not affect the linearity of the calibration curve (Supporting Information 6.3). For related studies, see: Livo, K.; Prasad, M.; Graham, T. R. Quantification of Dissolved O_2 in Bulk Aqueous Solutions and Porous Media Using NMR Relaxometry. *Sci. Rep.* **2021**, *11* (1), 290.

(27) Single-electron oxidation pathway by *m*CPBA can also be ruled out as Fenton-type oxidation reactivity was not observed under reaction conditions. See: Qiu, Y.; Hartwig, J. F. Mechanism of Ni-Catalyzed Oxidations of Unactivated C(sp^3)–H Bonds. *J. Am. Chem. Soc.* **2020**, *142* (45), 19239–19248.

(28) A similar mechanism via a second hydride transfer step of a similar adduct intermediate was proposed in the aminoxyl-mediated α-C–H oxidation of carbamates. See reference 12a.

(29) Zhu, Q.; Gentry, E. C.; Knowles, R. R. Catalytic Carbocation Generation Enabled by the Mesolytic Cleavage of Alkoxyamine Radical Cations. *Angew. Chem. Int. Ed.* **2016**, *55* (34), 9969–9973.

Table of Contents

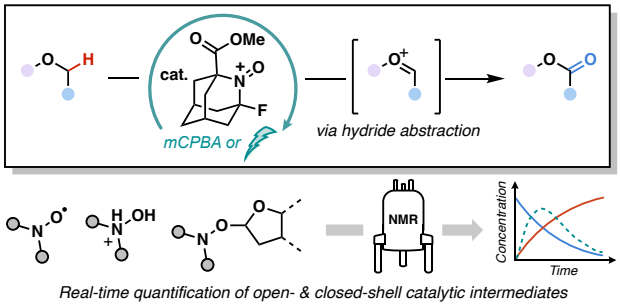

Real-time quantification of open- & closed-shell catalytic intermediates